PLANETARY RADIO EMISSIONS FROM HIGH MAGNETIC LATITUDES: THE "CYCLOTRON MASER" THEORY

D. Le Quéau

CRPE–CNET/CNRS – (LP 1010)
3, avenue de la République,
92131 Issy–les–Moulineaux, France

Abstract

Using the framework of the Cylotron Maser Instability we describe here theoretically some properties of the Jovian DAM, of the Saturnian Kilometric Radiation and of the Terrestrial, Auroral Kilometric Radiation.

A focus will be put on the determination of the spectral flux density emanating from each object and on the source structure.

The Jovian case is shown to be likely simpler than the Saturnian or terrestrial one, in which the magnetospheric gradients (of magnetic field, density and temperature) play an important role.

In all cases the maximum intensity of the observed emissions is consistent with the limitation of the wave growth by a trapping type saturation process.

Recent in situ measurements of the AKR sources allow us to understand schematically how the medium can act as a LASER for the excited waves, thus leading to an emission with a very small bandwidth, as observed.

NOMENCLATURE AND DEFINITIONS

$\perp$, $\parallel$	(subscripts) parallel, perpendicular to the planetary B–field
h,c	(subscripts) linked to the energetic (respectively cold) electron component
B	Planetary magnetic field, locally confounded with the vertical in the source region
p	Momentum of electrons $[p_\parallel, p_\perp, \phi = \tan^{-1}(p_y/p_x)]$
Γ	Lorentz factor $[1 + (p/mc)^2]^{1/2}$
$\beta_{\parallel,\perp}$	Electron velocity, normalized to the velocity of light
$W_{\parallel,\perp}$	Typical kinetic energy of the emitting electrons
δ	$W_\perp/mc^2$
$\beta_{\parallel 0}$	Typical parallel velocity of the emitting electrons
f	Electron distribution function
F	Electron distribution function averaged over $p_\parallel$ and ϕ
$n(n_h,n_c)$	Electron density (energetic, cold component)
ω, (ν)	Wave pulsation (frequency)
Ω_c	Electron gyropulsation
ν_{cp}	gyrofrequency at the foot of an emitting field line
ω_p $(\omega_{ph}, \omega_{pc})$	Electron plasma frequency
ε $(\varepsilon_h, \varepsilon_c)$	$(\omega_p/\Omega_c)^2$
$\Delta\omega$, $(\Delta\nu)$	Bandwidth of the emitted waves
θ	Angle between the wave vector and B
$N_{\parallel,\perp}$	Refractive indexes
θ_∞	Emergence angle of a wave, in an inhomogeneous medium
$\Delta\theta$	Width of the emission cone
W_{em}	Density of electromagnetic energy
V_g	Group velocity
γ	Temporal growth rate
ξ	Spatial (convective) growth rate $(\xi v_g/c\Omega_c)$
$L_{\parallel,\perp}$	Typical size of the source
D	Distance from the source
S_ν	Spectral flux density (in W m^{-2} Hz^{-1})
T_b	Brightness temperature
Λ	Inhomogeneity parameter
R_p	Planetary radius
Ψ	Relative phase between a rotating right handed electric field and the electron gyromotion
$N_\parallel$	Altitude range over which the phase changes by π (normalized to the parallel wave length)
ρ	Polarization ratio

1. Introduction

Four highly magnetized planets (Earth, Jupiter, Saturn and Uranus) are now known to emit non–thermal magnetospheric radio emissions. These radiations, which occur at various wavelengths (kilometric range for Earth (AKR) and Saturn (SKR), decametric to hectometric range for Jupiter (DAM and HOM)), are astonishingly powerful in comparison with the various energetic phenomena which are known to occur within the planetary environment. Despite their evident differences, which are likely due to the various magnetospheric morphologies, all these radiations exhibit strong observational similarities:

1. As far as they have been localized, the sources of AKR, SKR and DAM are found at high magnetic latitudes, in regions where energetic electron precipitations are observed sometimes in conjunction with the radio emissions. These regions are proved or suspected to be relatively depleted and highly magnetized, such that the ratio $\varepsilon = (\omega_p/\Omega_c)^2 \ll 1$.

2. The most intense component of these strongly polarized emissions is believed to be in fast extraordinary X–mode and generated at frequencies lying very close to the local gyrofrequency.

3. The dynamical spectra of all these radiations are finely structured in both frequency and time.

The details of the observational background will be presented in other reviews of this issue (Review papers of A. Boischot and H. de Feraudy et al.). They also have been extensively discussed in recent reviews (Genova, 1986, 1987a; and references therein).

All these similarities lead to the view that these radiations are likely due to the same fundamental mechanism. Various physical processes have been advocated so far as being responsible for the wave generation. These include linear conversion processes (Oya, 1974), non linear three–waves up–conversion (Roux and Pellat, 1979; Goldstein et al., 1983), radiation from cavitons (Galeev and Krasnosel'skikh, 1976; Cole and Pokhotelov, 1980), and linear instabilities (Melrose, 1976; Wu and Lee, 1979).

At this time, the most promising candidate for explaining the planetary radio emissions is a linear instability process, the Cyclotron Maser Instability (CMI hereafter). Since the pioneering work of Wu and Lee (1979), many papers have been devoted to this mechanism, such that real improvements have made concerning its ability to explain various observational features of the emissions (see the recent review by Wu, 1985).

In this process, the escaping radiation which is mainly a strongly polarized X mode, is directly amplified by a gyroresonant interaction between the right handed component of the electric field of the wave and a population of energetic electrons exhibiting an inversion of population in perpendicular energy. The great popularity of the CMI rests on the facts which have been quoted above. Furthermore, when in situ measurements of the sources are available (in the AKR case), such non thermal distribution functions have

been observed, sometimes at the place and at the moment at which the emissions are thought to be generated (Mizera and Fennel, 1977; Omidi and Gurnett, 1984). Finally, being a direct emission process, the CMI has a rather strong efficiency and thus can lead to high wave amplitudes, whatever the way by which this instability saturates (Wu et al., 1981a; Pritchett, 1986; Le Quéau et al., 1984a, 1985; Zarka et al., 1986).

The aim of the present paper is to discuss the various scenarios which could explain some observed features of the planetary radio emissions by using the theoretical framework of the CMI. It will focus, in each case (e.g. AKR, SKR and DAM which are at present better documented than the Uranian emissions), on the theoretical determination of the spectral intensities of the main part of the emissions. Incidentally, in the AKR case, where the plasma conditions prevailing in the sources are better known, we will also discuss the way by which the CMI could predict some spectral features of the radiation and the very tiny bandwidth which has recently been observed.

After this introduction, part 2 will be devoted to the presentation of the "conventional" CMI theory, and to an application of this process to the Jovian DAM. In part 3 we will discuss the role played by the inhomogeneity of the magnetospheric B–field in the emission process, with an application to SKR. Part 4 is concerned with the AKR, for which in situ observations of the source necessitate refinement of the theory. Finally, the conclusion will present some paths for further work.

2. Conventional CMI theory and the Jovian DAM

2.1 Basic instability process

Fundamentally, the CMI can be regarded as the "natural" instability of an homogeneous (hence non propagating) electric field which rotates, in the right handed sense, with respect to a static B–field, in the presence of an energetic population of gyrating electrons. When this population exhibits an inversion of population in perpendicular energy the CMI starts, thus leading to the amplification of the E–field (Schneider, 1959). For such a spatially homogeneous, time dependent E–field (E(t)) the Maxwell equations reduce to the balance between the conduction and displacement currents,

$$\frac{\partial \vec{E}}{\partial t} = \frac{ne}{\varepsilon_0} \int \frac{\vec{p}}{\Gamma} f d^3p \tag{1}$$

when the Vlasov equation is simply written:

$$\frac{\partial f}{\partial t} + \frac{\Omega_c}{\Gamma}\frac{\partial f}{\partial \phi} - e\vec{E}\frac{\partial f}{\partial \vec{p}} = 0 \tag{2}$$

After a linearization and a Fourier transform in time, one gets the dispersion equation for the R.H. electric field (which corresponds to a linear wave at its cutoff frequency):

$$G(\omega) = \frac{\omega_p^2}{\omega^2} \int d^3p_\perp p_\perp \frac{\partial f_0}{\partial p_\perp} \left(\Gamma - \frac{\Omega_c}{\omega}\right)^{-1} = 1 \tag{3}$$

where f_0 is the initial distribution function. Equation (3) exhibits the fact that the CMI can in some respect be considered as a resonant wave particle process. Resonant electrons have relativistic energies $W = \Gamma mc^2$ such that $\Gamma = \Omega_c/\omega$ and instability is clearly associated with an inversion of population of the perpendicular momentum distribution. Following this interpretation one sees that the real part of the frequency must be lower than the electron gyrofrequency, which precludes this simple theory from explaining an instability at the X mode cutoff frequency $\omega_x \sim \Omega_c(1+\varepsilon)$. Recently, Equation (3) has been analytically solved (Louarn et al., 1987). The electron population is assumed to be a mixing of a cold Maxwellian one (n_c) together with an energetic, non thermal one (characterized by a Dorris–Guest–Harris distribution function and a density n_h). It is there shown that, if $n_c/n_h \geq 10^{-2}$, the usual cold plasma X mode is indeed stable at its cutoff.

To allow the waves to propagate at right angle with respect to the magnetospheric field line does not change essentially the instability process and the dispersion equation is written:

$$G(\omega) = (1 - N_\perp^2)/(1 - N_\perp^2/2) \tag{4}$$

where $N_\perp$ is the perpendicular refraction index. When $n_c/n_h \geq 10^{-2}$ the unstable modes are "trapped" in the sense that they do not connect with the cold plasma X mode branch and thus cannot escape directly out of the generation region (Fig. 1) (Strangeway, 1985).

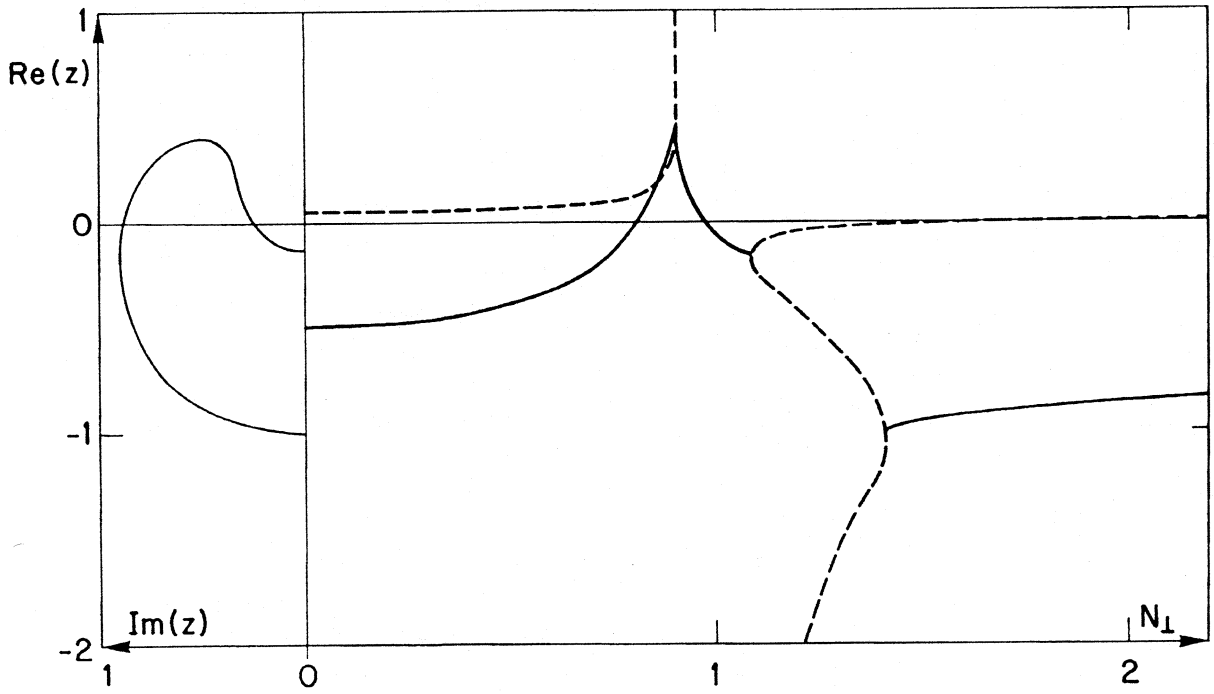

Fig. 1: Unstable "trapped" mode (full line) which does not connect to the other stable branches (dashed lines). Equation (4) is solved with $n_H/n_c \sim 5\%$. The electron distribution function is here taken to be a Dirac's function peaked at $p_\parallel = 0$ and $p_\perp = \sqrt{2\delta}mc$ with here $\delta \sim \omega_{ph}^2/\Omega_c^2$. The right panel shows the real dispersion (e.g. $R_e(z)$ vs $N_\perp$ where $z = (\omega - \omega_c)/\omega_c\delta$ and $N_\perp$ is the perpendicular refractive index. The left panel shows the growth rate (e.g. Im(z)).

Thus, if the planetary magnetospheric plasma is fed by a substantial amount of cold electrons, the CMI can only excite freely escaping X–modes when these modes have a finite parallel wave vector $k_{\|}$. If, at the same time, the inversion of population occurs at a finite parallel velocity, $\beta_{\|0}$, the unstable frequency range can be Doppler shifted above the cutoff frequency of the cold X–mode, which allows freely escaping waves to be directly emitted.

These are the main physical concepts underlying the "conventional" CMI theory (Figure 2). The dispersion equation of the X mode is roughly determined by the cold magnetoionic theory, and the growth rates are obtained by perturbation of this equation by the non hermitian part resulting from the contribution of the resonant electrons. These verify the usual resonance condition

$$\omega - \frac{\Omega_c}{\Gamma} - k_{\|} v_{\|} = 0 \tag{5}$$

Table 1 (next page) summarizes the main characteristics of the "conventional" CMI theory, including the choice of parameters which optimizes the wave amplification (Le Quéau et al., 1984a,b).

According to this linear theory the fundamental ($\omega \sim \Omega_c$) X mode, which is the main component of the radiation, must be emitted within a very thin conical sheet which has a semi apical angle lying very close to 90°.

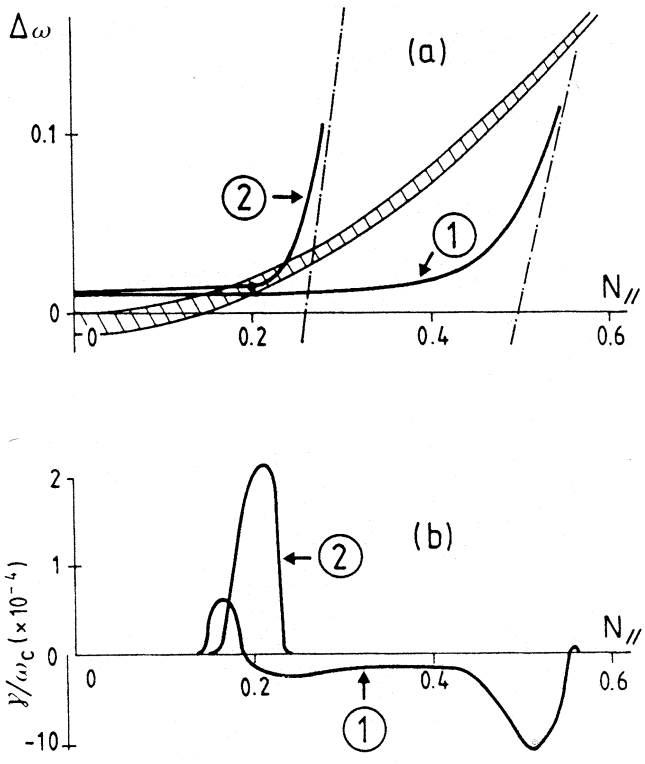

Fig. 2: "Conventional" CMI. The wave dispersion curves (1 or 2) closely follow the cold plasma ones. When the propagation angle is "adapted", case 2, the curve enters the instability zone (hatched area) without further attenuation. Here $\Delta\omega = (\omega - \omega_c)/\omega_c$ and $N_{\|}$ is the parallel index of refraction.

Table 1

Estimated characteristics of the most unstable X mode in the conventional CMI theory ($\varepsilon_c \ll 1, \varepsilon_h \ll 1, \delta \ll 1$)

Optimizing conditions:	$\beta_{\parallel 0} \sim N_{\parallel} \sim 2\varepsilon_c^{1/2}; \delta \sim \varepsilon_c^{2/3}\varepsilon_h^{1/3}; N_{\perp} \sim 0.7$
Frequency of the wave:	$\omega \sim \Omega_c(1 + 2\varepsilon_c)$
Temporal growth rate:	$\gamma/\Omega_c \sim \varepsilon_h^{2/3}\varepsilon_c^{1/3}$
Spatial growth rate:	$\xi_{\perp} \sim \varepsilon_h/\delta$
Angle of propagation:	$\theta \sim \pi/2 - 2^{3/2}\varepsilon_c^{1/2}$
Instantaneous bandwidth:	$\Delta\omega/\omega \sim \delta$
Width of the emission cone:	$\Delta\theta \sim \sqrt{2}\{(4\varepsilon_c + \delta)^{1/2} - (4\varepsilon_c)^{1/2}\}$

2.2 Limitation of the wave amplitude

The linear theory does not allow directly the determination of the wave amplitude and thus the spectral flux density of the emission. Two different types of processes could lead to such a limitation of the emitted intensity:

1. The free convection of the electromagnetic energy out of the finite size source leads to an intensity proportional to the gain factor $\exp(2\gamma\tau_c)$ where $\tau_c \sim L_{\perp}/V_g$ is the time spent by the wave energy to pass through the source, which has a perpendicular extension $L_{\perp}$.

2. If the wave electric field is allowed to reach a sufficient level, non linear saturation processes can stop the wave growth, at least if it occurs on a time scale smaller than τ_c.

Since the CMI is a resonant wave–particle process, essentially two different types of non linear phenomena are expected to occur (Le Quéau and Roux, 1987):

1. If the spectral bandwidth of the emission is small (e.g. if $(\Delta\omega)^{-1}$ is larger than both the evolution time of the wave amplitude and of the electron distribution), the wave is felt by the electrons as being quasi monochromatic and a coherent trapping type saturation process occurs. The resulting electromagnetic energy density is obtained by matching the trapping frequency to the temporal growth rate which roughly gives:
$$W_{em} \approx (\varepsilon_h/4)(n_h \delta m c^2) \tag{6}$$

2. Conversely, if the spectral bandwidth is sufficiently broad, energetic electrons feel an incoherent wave bath and suffer stochastic motions which lead to the quasilinear diffusion of the non thermal part of the distribution function. As the parallel velocities of the electrons remain constant during these motions, the diffusion only concerns the perpendicular velocities of the electrons. Thus the distribution function must finally be "plateaued" over the velocity range at which the inversion of population

initially takes place. This allows an estimate of the electromagnetic energy density which can be furnished to the medium if all the quasilinear process has time to occur before the wave energy is evacuated out of the source:

$$W_{em} = 2\pi n_h/m \int_0^{p_0} p_\perp dp_\perp \int_0^p p'_\perp dp'_\perp \{F_0(p', \infty) - F_0(p', 0)\} \quad (7)$$

$$W_{em} \sim 5 \cdot 10^{-2} (\delta n_h m c^2) \quad (8)$$

In (7) F_0 is the electron distribution function, averaged over both the momentum angle θ and the parallel momentum $p_\parallel$, respectively at the start time of the CMI (t = 0) and at the end of the whole process (t = ∞). $F_0(p_\perp, \infty)$ must then be constant for $p_\perp < p_0$ and roughly equal to F_0 ($p_\perp$, 0) for $p_\perp > p_0$, where p_0 is determined by the conservation of the number of electrons in velocity space. The estimate (8) is done by using a DGH function for modelling $F_0(p, 0)$. It leads to considerably higher fluxes than the trapping estimate (6) because the quasilinear process allows all the free energy available in the initial distribution function to be finally transformed into electromagnetic energy. Such an estimate obviously assumes that all the quasilinear processes have time to occur before the convection of the waves out of the source and before the replenishment of the free energy source by new particle precipitations.

2.3 An application to the generation of the Jovian DAM

The DAM sources are unfortunately poorly known and a lot of uncertainties remain concerning the plasma conditions prevailing in such regions. We will thus restrict our investigation to the higher frequency DAM range ($\nu \sim 40$ MHz) which is expected to be generated in the immediate vicinity of the planet, at the foot of the Io flux tube (IFT), which is the only place where a cyclotron frequency $\nu_{cp} = 40$ MHz is available within the Jovian magnetosphere. The electron density is also better known there than in any other place: As shown by radio–occultation experiment, ω_p must be of the order of 3 MHz ($n_c \sim 210$ cm^{-3}). This is substantial and permits the assumption that the wave propagation could be supported by this cold population and thus that the conventional CMI works. The density ratio between the cold and energetic population is still unknown and will be taken $n_h \sim 0.1\ n_c$ as a reasonable supposition. Finally the flux density at the Earth can be written:

$$S_\nu = (N_\perp c W_{em}) \left(\frac{L_\perp L_\parallel}{D^2} \right) \quad (9)$$

The wave energy is supposed to be convected at right angle to the Jovian magnetic field and the source size is defined by $L_\perp \sim \eta D_{Io}/\sqrt{5}$ (a fraction η of the extension of the IFT at the planetary surface) and $L_\parallel = (\nu \partial/\partial z(\log B))^{-1}$ is the vertical extension over which the gyrofrequency (and thus, roughly, the emission frequency) varies by 1 Hz. D $\sim$ 4 AU is the Earth–Jupiter mean distance. The results are summarized in Table 2.

The waves are emitted at large angle from the local B field and are expected to exhibit a significant amount of linear polarization (polarization ratio $\rho \sim 0.2$). As the growth rate is large, the gain factor could reach huge values ($\exp(4 \cdot 10^3 \eta)$!). This leads one to

suspect that if the source size is not very small (larger than a few kilometers) non linear saturation processes are likely to occur.

It is worthwhile to note that the quasilinear saturation process leads to flux densities which are many orders of magnitude above the observed values. Conversely, the trapping process directly leads to a reasonable estimate (Carr et al., 1983). Thus, if the CMI is the mechanism which generates such an emission, either the source size is very small or the quasilinear saturation process is rapidly quenched, or, finally, trapping saturates the instability process.

Table 2:

Emission of Jovian DAM by the "conventional" CMI theory
(optimization of the growth rate like in Table 1)

Frequency of emission: $\nu \sim \Omega_c/2\pi \sim 40$ MHz
Estimated values of $\varepsilon_c \sim 5.6 \cdot 10^{-3}$ and $\varepsilon_h \sim 5.6 \cdot 10^{-4}$
Typical energy of emitting electrons: $W_\perp = mc^2\delta = 1.3$ keV
$W_\parallel = 2mc^2\varepsilon_c = 5.6$ keV
Emission lobe: $\theta \approx 78°$; $\Delta\theta \approx 1°$
Polarization ratio: $\rho = 0.2$
Growth rate (temporal): $\gamma/\Omega_e \sim 1.2 \cdot 10^{-3}$; $\gamma^{-1} \sim 3 \cdot 10^{-6} s$
Estimated bandwidth (linear): $\Delta\omega/\gamma \sim 2$ [$\Delta\nu \sim 10^5$ Hz]
Propagation time out of the source: $L_\perp/V_g \sim 7 \cdot 10^{-3} s$

Flux density and mean brightness temperature
(averaged over the Jovian disk)

Q. Linear theory	Trapping
$S_\nu = 1.5\eta \cdot 10^{-16} W m^{-2} Hz^{-1}$	$S_\nu = 4.5\eta \cdot 10^{-19} W m^{-2} Hz^{-1}$
$T_b = 7\eta \cdot 10^{15} K$	$T_b = 2\eta \cdot 10^{13} K$

3. Inhomogeneity effects: an application to SKR

3.1 Wave amplification in an inhomogeneous plasma: the linear transfer

The "conventional" CMI only excites fundamental X modes at frequencies lying very close to the cutoff frequency ω_x. For such frequencies even a very small gradient of the plasma parameters (B or n_c) will permit a very rapid change of the wave vector. Thus the wave refraction drastically limits the size of the region over which a resonant condition such as given by (5) can be realized for a given set of electrons. Specifically, by taking into account the B field inhomogeneity only, which is the main inhomogeneity governing the wave propagation in such largely depleted regions, the resonance can only be maintained over an altitude range (normalized to the parallel wave length)

$$N_\parallel \approx \frac{16}{3}\Lambda^{1/2}\varepsilon_c^{5/4} \tag{10}$$

where $\Lambda = R_p\nu/c(\nu_{cp}/\nu)^{1/3}$ characterizes the dipolar B–field gradient: R_p is the planetary radius and ν_{cp} the gyrofrequency at the foot of the emitting field line. Over this altitude range, the relative phase Ψ between the rotating electric field of the wave and the electron gyromotion varies indeed significantly ($\Delta\Psi \approx \pi$).

Application of (10) to the parameters, suspected to correspond to both the AKR and the SKR generation, leads to $N_\parallel \leq 1$ which necessitates a modification of the conventional CMI theory in order to take into account the resonance detuning linked to the B–field inhomogeneity (Le Quéau et al., 1985; Zarka et al., 1986). It can be shown that:

1. The electrons which interact most efficiently with the wave must fulfill both conditions $\Psi' = 0$ and $\Psi'' = 0$ (where $'$ means the derivative with respect to altitude z). The interaction length is of the order of $\Delta z \sim (\Psi''')^{-1/3}$. Conversely a given wave can interact with an extended set of electron velocities which is closely linked to the whole altitude range over which the wave can interact with the unstable electron distribution (Figure 3).

2. For $\varepsilon_c \geq 0.148$ the coupling is impossible and thus the CMI cannot take place.

3. For $\varepsilon_c \leq 0.148$ the angular domain, over which the X mode is destabilized, is very limited and localized around an angle θ_∞ (such that $\cos(\theta_\infty = \sqrt{2}\varepsilon_c^{1/4})$), where θ_∞ is the angle of propagation of the wave, outside the very small source region.

4. Due to the wave refraction the expected source size is very small

$$\begin{aligned} L_\parallel &\sim \frac{2^{3/2}}{5}\delta^{1/2}\varepsilon_c^{1/4}R_p\left(\frac{\nu_{cp}}{\nu}\right)^{1/3} \\ L_\perp &\sim L_\parallel/\varepsilon_c^{1/4} \end{aligned} \tag{11}$$

   where $L_\parallel$ ($L_\perp$) is the vertical (latitudinal) extension of the source.

5. Finally the flux density emanating from the plasma can be determined by a linear transfer equation:

$$S_\nu = 2\pi/D^2 \int_{-\infty}^{\infty} ds P(s) \exp\left\{\int_S^\infty \xi(s')ds'\right\} \tag{12}$$

   where P(s) is the incoherent power flux due to the extraneous currents, $\xi(s)$ the local convective growth (or damping), and s the abscissa along the ray path. The mathematics which allow the determination of P and ξ is rather tedious (see Eq. 21 and 22 of Zarka et al., 1986) but finally all the quantities appearing in (12) can be determined from the electron distribution function (Figure 3). This process is simply a linear transfer of the wave energy throughout the amplifying plasma medium. The B–field inhomogeneity naturally limits the source size and allows the power flux to remain finite (unlike the homogeneous calculation in which a finite source size must be independently fixed).

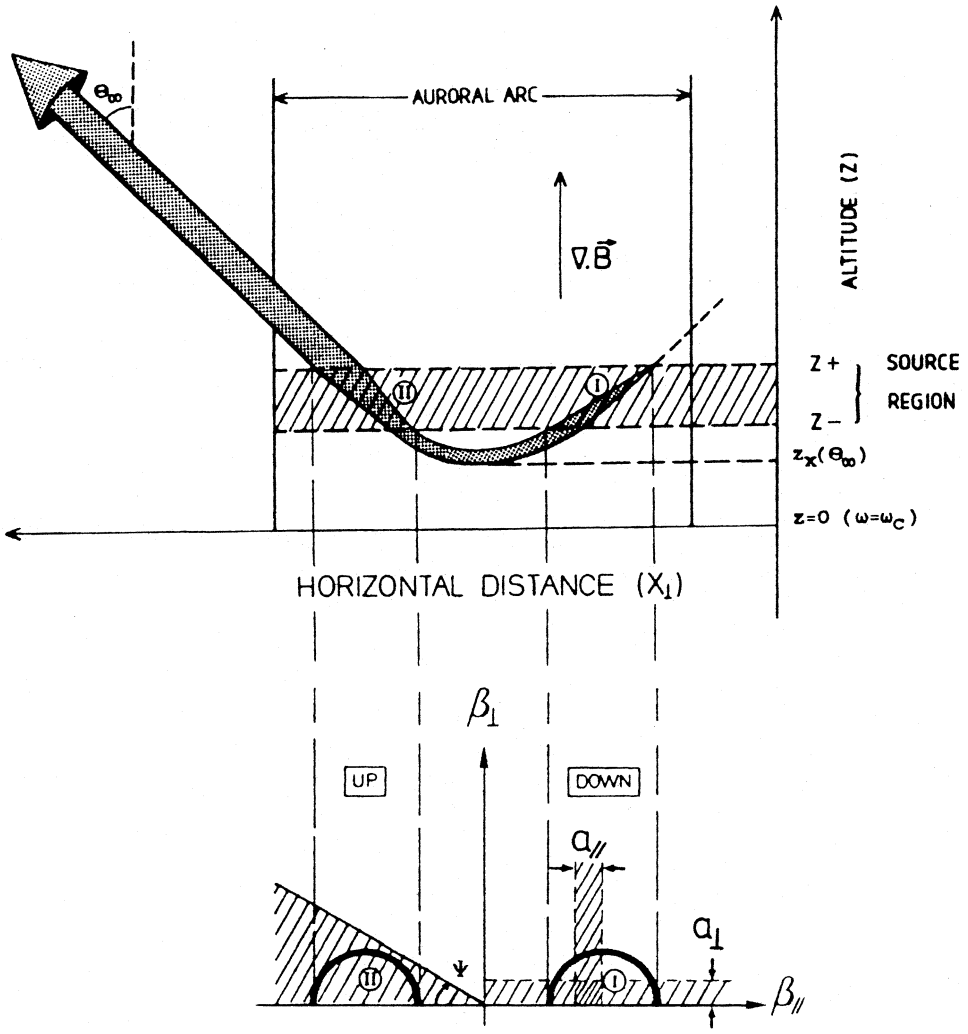

Fig. 3: Inhomogeneous source model. It is characterized by the vertical magnetic field gradient $\nabla|B|$. As it propagates and refracts, a given wave, determined by its emergence angle θ_∞, first interacts with the downgoing electrons (region I in the velocity plane) then with the upgoing ones (region II). There is a one to one correspondence between these two regions and the altitude range $\Delta z = z^+ - z^-$ delimiting the source.

3.2 Non linear saturation processes

If the gain is sufficient, the wave level can reach larger values such that the non linear detuning process can stop the wave growth. As these processes are also resonant wave particle phenomena, they will also be strongly modified by the B–field inhomogeneity. Specifically, when the wave electric field becomes high enough to allow the trapping period to be of the order of the wave particle interaction time, then the trapping mixing phenomenon is expected to quench the instability (Le Quéau and Roux, 1987). Depending of the values of both ε_c and the inhomogeneity parameter Λ the maximal electromagnetic energy available can thus be estimated (Galopeau et al., 1987):

$$W_{em} \sim \varepsilon_0 \left(\frac{m\omega_c}{e}\right)^2 \delta^{-1}\Lambda^{-8/3} \quad if \quad \Lambda^{1/3}\delta^{1/2} \geq 2 \tag{13}$$
$$W_{em} \sim \varepsilon_0 \left(\frac{m\omega_c}{e}\right)^2 \Lambda^{-2} \quad if \quad \Lambda^{1/3}\delta^{1/2} \leq 2$$

Using (13) and the known size of the source (9) the spectral flux density at distance D can be determined

$$S_\nu = \frac{1}{3\sqrt{2}} \frac{cW_{em}}{\nu} R_p \left(\frac{\nu_{cp}}{\nu}\right)^{1/3} \frac{L_\perp^2}{D^2 L_\parallel} \tag{14}$$

3.3 Maximum flux densities of the SKR

The SKR is likely to be emitted in high magnetic latitude regions, which coincide with the two dayside Saturnian cusps (Lecacheux and Genova, 1983).

As far as we know, the cold plasma content is expected to be small in these regions, except in the immediate vicinity of the Saturnian surface. Voyager measurements indeed led to the conclusion that the inner magnetospheric plasma of Saturn is mainly fed by two sources (Lazarus and McNutt, 1983):

1. The ionosphere which can be modelled by hydrostatic equilibrium with a scale height h_{ion}

$$n_{ion} = n_{ion}^0 \exp[-(R - R_S)/h_{ion}] \tag{15}$$

   where R is the distance from the planet center, R_S the Saturnian radius, $n_{ion}^0 \approx 2{\cdot}10^4$ cm^{-3} and h_{ion} has been estimated to be of the order of 0.01 to 0.02 R_S, near the equatorial plane.

2. A plasma disk, due to the centrifugal confinement of the plasma near the equatorial plane, which can be modelled as

$$n_{disk} = \frac{n_{disk}^0}{L^3} \exp[-(R\cos(X)/h_{disk})^2] \tag{16}$$

   where X is the azimuthal angle from the axis of rotation and L the McIlwain's parameter. Scale heights $h_{disk} \approx 0.25$ to 1 R_S have been observed during the Voyager–Saturn closest approach and $n_{disk}^0 \approx 2{\cdot}10^3$cm^{-3}.

Finally, the Saturnian magnetic field appears to be quite perfectly dipolar and aligned with the rotation axis.

This very simple magnetospheric model foresees that the expected SKR sources are very depleted ($\varepsilon_c \approx 10^{-3}$ to 10^{-5} along the Saturnian field line emerging at the latitude 75° (L ≈ 15)), such that, according to (10), $N_{\parallel}$ must be < 1. It is thus tempting to use the above quoted inhomogeneous CMI theory and try to relate the theoretically determined flux densities with the observed ones.

A first step in that direction has been done recently (Galopeau et al., 1987). In this work the maximal flux densities expected from the trapping type saturation process in inhomogeneous media (13), has been determined (Figure 4). It is obvious that this modelling conveniently fits the data: as expected, the calculated spectrum, which is thought to give the maximal flux expected at each frequency, effectively envelops the observed spectra. The chosen input parameters of this calculation are $h_{ion} \approx 0.05\ R_S$, $h_{disk} \approx 0.7\ R_S$ and $\delta mc^2 \approx 1$ keV, which is of the order of the energy of the precipitating electrons (10 keV), as inferred from the UV observations of the Saturnian auroral glow (Sandel et al., 1982). The slow decrease of the spectrum at low frequencies is essentially due to the decrease of the source size with ε_c, as expected from (11). The abrupt drop–out at high frequency is linked to the fact that the CMI no more works when $\varepsilon_c \geq 0.148$.

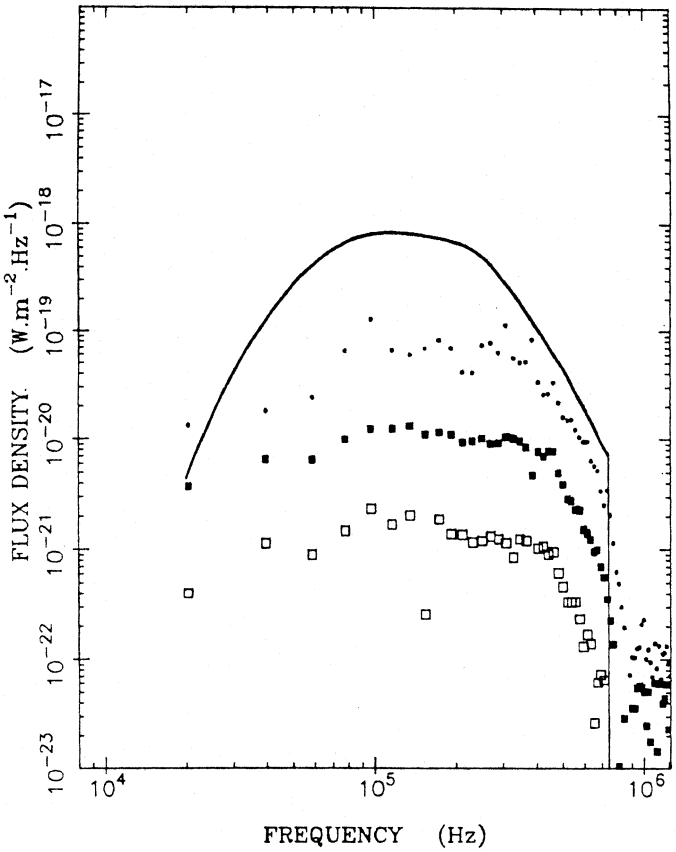

Fig. 4: Comparison between the theoretically determined, maximal, SKR spectrum with flux density observed 50% (□), 10% (□) and 1% (•) of the time (Voyager data). Right handed polarization has been here chosen and the total observation time is about one day. Fluxes are normalized to 1 AU (see text).

4. The generation of auroral kilometric radiation

4.1 The MASING scenario

Since its discovery by Benedictov et al. (1965), AKR has been the subject of many observational investigations, including both remote sensing and in situ measurements, which put more severe constraints on the emission scenario than for any other planetary radiation. It is now well established that AKR is emitted in conjunction with discrete auroral arcs, in regions where $\varepsilon \ll 1$. Since the wave length is kilometric and the Earth's radius far smaller than the Saturnian one, $N_{\|}$ is very small, and the inhomogeneous CMI theory can be used, if one assumes that the energetic plasma component is sufficiently weak for the wave propagation to be only determined by the cold plasma component alone, a point which needs further discussion. Figure 5 gives an example of such a calculation using both the linear transfer Equation (12) (the crosses) and non linear saturation arguments (the grey zone in the upper part of the figure) (Zarka et al., 1986). Here the parameter ε_c is optimized, for each value of the electron parallel energy, such that the flux is maximized: ε_c ranges from $2{\cdot}10^{-3}$ for $W_{\|} \sim 10$ keV to $6{\cdot}10^{-3}$ for $W_{em} \sim 20$ keV. These flux densities are here compared with the data range provided by remote observations of AKR. It is seen that, with the exception of the strongest AKR event ever reported in the literature (Gurnett, 1974), the observations are consistent with a non saturated emission. It should be noticed that the electron energies which are needed here are rather large as compared with those which are usually recorded during inverted V events.

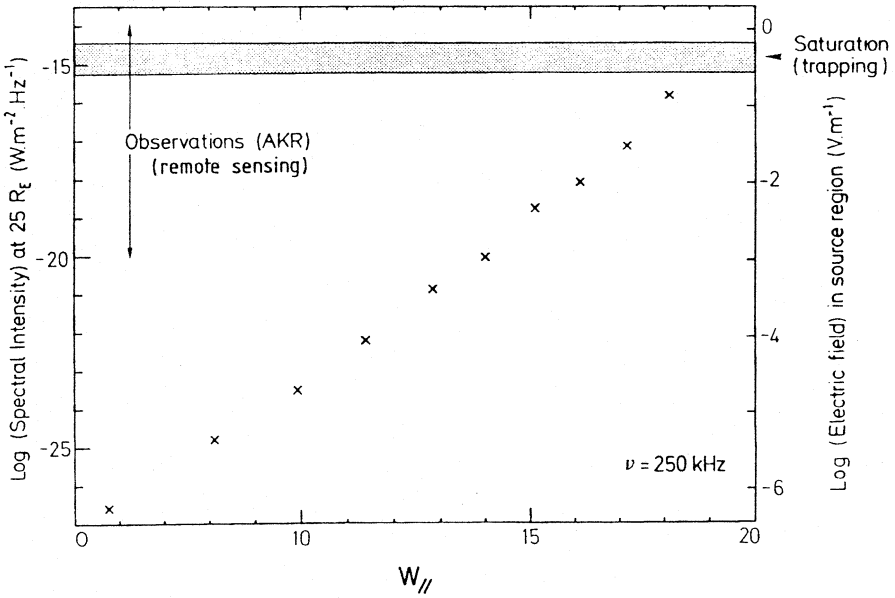

Fig. 5: Computed spectral intensities at 25 Earth's radii, for a 250 kHz AKR emission. Crosses show the linear transfer results, using an electron distribution function resembling to those sketched in Figure 3 (Hole–like feature with loss–cone). The grey shaded area indicates the intensity determined by assuming that the instability is saturated by trapping process. As a comparison the range of observed AKR intensities is shown. $W_{\|}$ is the parallel energy of the emitting electrons (Hole–like feature).

Finally the source size of AKR can be estimated from (11): $L_{\parallel} \sim 20$ km, $L_{\perp} \sim 100$ km. As seen by a remote observer, and depending on the viewing geometry, the size of the source thus lies in the myriametric range. This simple MASING model foresees source extensions which are not far from those inferred by interferometric measurements (Baumback et al., 1986).

4.2 The search for a LASING scenario

As observed from remote sensing, the AKR dynamical spectrum virtually always consists of very fine drifting spectral lines (Gurnett et al., 1979a). An estimate of the AKR minimal bandwidth has been tried recently (Baumback and Calvert, 1987): an instantaneous bandwidth as low as 10 Hz has been found. This result evidently put a drastic constraint on the generation mechanism, and it is interesting to determine the size of the minimum bandwidth predicted by the CMI.

The overall relative bandwidth of an emission due to a MASING source will be of the order of $L_{\parallel}\partial/\partial z(\parallel Log\ B \parallel)$. Thus $\Delta\nu/\nu \approx 5 \cdot 10^{-3}$ which is far larger than measured. It is thus necessary to turn towards the LASER concept first proposed by Calvert (1982).

If for some reasons, the emission process is able to select one among all the possible unstable modes then the bandwidth of the emission will be finally determined by the phenomena which ultimately limits the coherence of the resonant wave–particle interaction which governs the CMI, i.e. the azimuthal trapping of the emitting electrons. It is thus expected that the minimum bandwidth will be given by the trapping frequency ν_T, and

$$\frac{\Delta\nu}{\nu} = \delta^{1/4} \left(\frac{eE}{mc\omega}\right)^{1/2} \tag{17}$$

For a 250 kHz emission, a 1 mVm^{-1} electric field and a perpendicular energy of 1 keV one obtains $\Delta\nu \approx 35$ Hz which is comparable with the 5 – 20 Hz bandwidth estimated by Baumback and Calvert (1987).

In order to understand how such precise mode selection can appear, it is necessary to consider the small scale spatial structure of the source. The observations performed by the ISIS satellite have already shown that strong latitudinal density gradients are expected there (Benson and Calvert, 1979). Recent in situ measurements by the VIKING satellite (de Feraudy et al., 1988, this issue) also show that the latitudinal extension of the AKR sources is very small and that, within these, the electron cold plasma component quite entirely vanishes and is replaced by an equivalent amount of energetic plasma (energies of the order of 5 keV). Moreover, during source–crossings, the lower cutoff of AKR falls near or even below the gyrofrequency, where it gently follows the cold plasma X mode cutoff when AKR is observed outside the source.

It is now well known from theoretical studies (Strangeway, 1985; Pritchett, 1986; Le Quéau and Louarn, 1987) that the presence of a dominant energetic population lowers the X mode cutoff, even below the gyrofrequency, in which case it can be unstable in purely perpendicular propagation (see Figure 1).

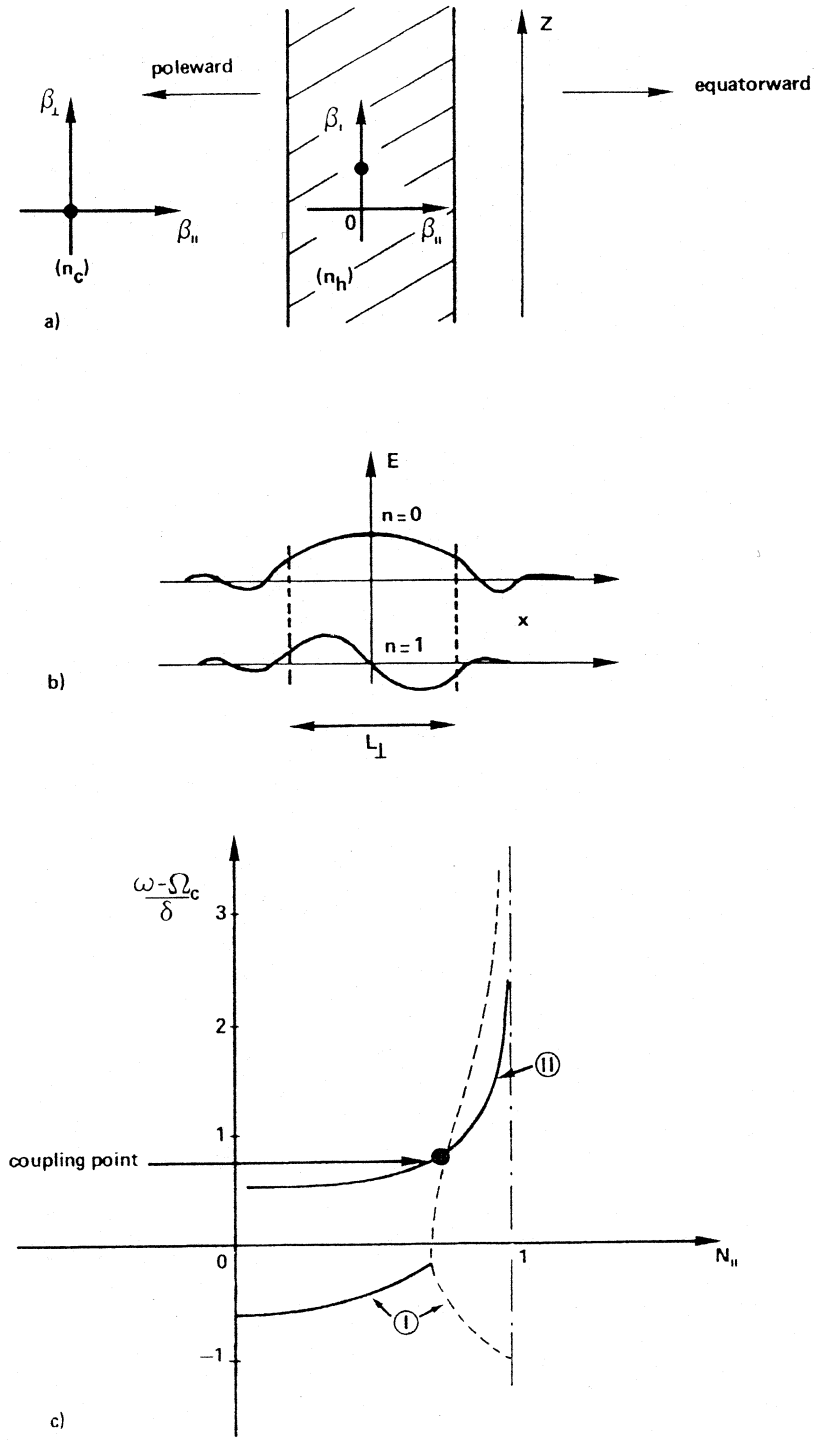

Fig. 6: Schematics of a LASER emission scenario. The source is a thin slice of energetic electrons, inserted over a limited latitudinal spatial range inside a colder plasma region (a). The discrete unstable modes, the perpendicular wave length of which are determined by the source extension, cannot propagate outside (b). But, by propagating upwards, they found a region where the coupling with the cold plasma mode (II) is possible (c). These internal modes (I) can be either unstable (—-) or stable (– –), depending on the altitude.

All these facts allow one to propose the following schematic view for the AKR generation.

The sources are small slices of energetic plasma (with a density n_h, and a with $L_\perp \approx$ a few tens of kilometers), imbedded into a cold plasma region (density n_c) which extends both poleward and equatorward from the source (Figure 6a). Within the slice unstable modes can be generated at frequencies lying around the gyrofrequency. They cannot escape freely in the cold surrounding plasma, in which the X mode cutoff frequency is higher.

Thus, taking into account the boundary conditions at the edges of the slice, a discrete set of modes can be destabilized which have quantized perpendicular wave lengths $\lambda_\perp(m) \approx 2L_\perp/m$ $(m = 0, 1, 2 \ldots)$. They also can have a small parallel wave vector which is essentially determined by the distribution function of the electrons (Figure 6b). The system thus acts as an active wave guide. Due to the finite $k_\parallel$ the electromagnetic energy can escape upwards. During the propagation $k_\parallel$ increases, such that, at some distance from the generation region, the wave crosses an altitude where the dispersion of the confined mode has exactly the same characteristics than the cold plasma X mode (Figure 6c). At this altitude the energy can finally be radiated away with propagating characteristics depending of all the process. Condition for the coupling point to exist is $n_h > n_c$, such that the AKR sources are likely to be fibers of hot electrons immersed within a more tenuous, colder region. If the fiber is sufficiently small then only a few modes can be destabilized thus leading to well separated discrete spectral components. This scenario also presents the advantage that the unstable modes are now destabilized in regions where purely energetic electrons are present, which enhance the growth rate as compared with the "conventional CMI theory", and likely allow a less energetic electron population to be sufficient for producing the observed fluxes.

5. Conclusions

At this time the CMI remains the most promising mechanism for explaining the generation of AKR, SKR and DAM.

In the Jovian case, the magnetospheric gradient length is likely to be so large as compared to the emitted wave length that a homogeneous theory can be used. It predicts that the waves are emitted at large angle from the local B–field. The measured values of the spectral intensities are consistent with a trapping type saturation mechanism.

The relative simplicity of the Saturnian magnetosphere allows one to model in a very simple fashion the essential plasma parameters which are needed for describing the wave amplification. Unlike the Jovian case, the inhomogeneity of the magnetospheric B–field is then expected to play an important role in the wave generation. Assuming that the saturation occurs through a trapping process, one can estimate the maximum flux expected to emanate from this object. This theoretical determination agrees very well with the observed characteristics of the mean spectra of SKR.

The richness of the observational data concerning the AKR necessitates a further improvement of the theoretical description of the sources. It is likely that both the vertical

gradients of the B–field and latitudinal gradients of the density and temperature of the plasma are essential ingredients for describing the emission scenario.

As in the Saturnian case, the B–field inhomogeneity must limit the wave gain and thus restrict the source size to the myriametric range.

Again, the inhomogeneous CMI theory gives a correct estimate of the spectral intensities observed as emanating from the auroral region.

In situ observations also show that the SKR source is characterized by strong perpendicular gradients of the plasma density and of the plasma temperature.

This allows one to understand schematically how such a medium can select and amplify well defined spectral modes, within the wave guide formed by the strong perpendicular density and temperature gradients at the edges of the sources.

The source will then be a slightly overdense slice of energetic electrons aligned with the geomagnetic field, imbedded within a colder plasma. The edges of such a structure act as mirrors for the modes which can be destabilized within the structure. This naturally leads to the excitation of discrete spectral modes which can only escape from this source region at an altitude which is slightly higher than the altitude of their generation. This crude model can explain simply the data recorded by the VIKING satellite during source crossings. A complete investigation of such a complex source model is nevertheless needed for determining more quantitatively if it could explain the observations.

It will in turn be interesting to use such a scenario in the case of SKR or DAM to see if some of the spectral structure of these radiations can be explained in that fashion.